

# HNCO abundances in galaxies: Tracing the evolutionary state of starbursts

Sergio Martín

smartin@cfa.harvard.edu

*Harvard-Smithsonian Center for Astrophysics, 60 Garden St., 02138, Cambridge, MA, USA*

J. Martín-Pintado

*Departamento de Astrofísica Molecular e Infrarroja, Instituto de Estructura de la Materia, CSIC, Serrano 121, E-28006 Madrid, Spain*

R. Mauersberger

*Instituto de Radioastronomía Milimétrica, Avenida Divina Pastora 7, Local 20, E-18012 Granada, Spain*

*Joint Alma Observatory, Av. El Golf 40, Piso 18, Las Condes, Santiago, Chile*

## ABSTRACT

The chemistry in the central regions of galaxies is expected to be strongly influenced by their nuclear activity. To find the best tracers of nuclear activity is of key importance to understand the processes taking place in the most obscured regions of galactic nuclei. In this work we present multi-line observations of CS, C<sup>34</sup>S, HNCO and C<sup>18</sup>O in a sample of 11 bright galaxies prototypical for different types of activity. The <sup>32</sup>S/<sup>34</sup>S isotopic ratio is  $\sim 10$ , supporting the idea of an isotopical <sup>34</sup>S enrichment due to massive star formation in the nuclear regions of galaxies. Although C<sup>32</sup>S and C<sup>34</sup>S do not seem to be significantly affected by the activity type, the HNCO abundance appears highly contrasted among starburst. We observed HNCO abundance variations of nearly two orders of magnitude. The HNCO molecule is shown to be a good tracer of the amount of molecular material fueling the starburst and therefore can be used as a diagnostics of the evolutionary state of a nuclear starburst.

*Subject headings:* ISM: molecules — galaxies: abundances — galaxies: ISM — galaxies: starburst — galaxies: Seyfert — radio lines: galaxies

## 1. Introduction

The nuclear regions of active galaxies can harbor different energetic phenomena such as starbursts (SBs) and Active Galactic Nuclei (AGN) which are responsible for producing the bright emission stemming from their central regions. The heating of the interstellar medium (ISM) in nuclei with different type of activity is expected to be dominated by a variety of mechanisms, such as UV, X-rays, and/or shocks, which will ultimately drive their observed chemical richness (Martín et al. 2006b, and references therein). Disentangling which of this mechanisms is the main power source of galactic nuclei is complicated by the high obscuration affecting these objects. This fact becomes critical in the case of Ultra Luminous Galaxies (ULIRGs) and high- $z$  sources. Therefore the observation of the dense molecular material has become an essential tool to get an insight in the evolution and classification of the nuclear activity in galaxies.

Finding appropriate molecular species to accurately trace each of these heating mechanisms is crucial to establish the nature of the central engine. Molecular species like HCN and  $\text{HCO}^+$ , and in particular the ratios HCN/CO and HCN/ $\text{HCO}^+$ , have been claimed to be appropriate to differentiate between the SB and the AGN contribution in galactic nuclei (Kohno et al. 1999; Kohno 2005; Krips et al. 2008). Similarly, species such as HNC and CN are thought to show enhanced abundances in extremely irradiated environments (Aalto et al. 2002, 2007). A dichotomy still remains concerning the different evolutionary state of nuclear starburst. While at an early stage, the heating of the ISM is thought to be dominated by shocks affecting the molecular clouds fueling the starburst, the late stages of starburst are vastly dominated by the UV radiation originated in the newly formed massive stars. This scenario has been inferred from the extensive observation of the prototype sources NGC 253 and M 82 in a number of key molecular tracers such as  $\text{SO}_2$ ,  $\text{H}_2\text{S}$ , OCS (Martín et al. 2003, 2005),  $\text{HOC}^+$ , and  $\text{CO}^+$  (Fuente et al. 2005, 2006). Unfortunately, these tracers are generally too faint to be detected, but for the brightest prototypical nearby galaxies.

In a recent observational study carried out towards a sample of molecular clouds dominated by different heating mechanisms within the Galactic center region (Martín et al. 2008), we have found that the CS/HNCO abundance ratio is highly contrasted between molecular clouds illuminated by the UV radiation from massive star clusters and the giant molecular cloud complexes shielded from photodissociation and mostly heated by shocks. The origin of the large changes in the CS/HNCO ratio is due to the enhancement of CS in photon-dominated regions (PDRs) through reactions involving  $\text{S}^+$  (Sternberg & Dalgarno 1995) as opposed to the highly photodissociable HNCO, which is destroyed by the UV photons. Both observations of photodissociation regions within our Galaxy and photochemical models show the suitability of CS as a PDR tracer (Goicoechea et al. 2006). In addition, HNCO is en-

hanced in the presence of shocks due to its injection in the gas phase from the grain mantles (Zinchenko et al. 2000). This paper presents a follow up study of the CS/HNCO ratio towards a sample of prototype galaxies with different nuclear activity. Although CS has been extensively observed in external galaxies (Baan et al. 2008), HNCO had only been detected in four galaxies prior to this work (Nguyen-Q-Rieu et al. 1991; Wang et al. 2004).

## 2. Observations and Results

Observations were carried out with the IRAM 30 m telescope on Pico Veleta, Spain, during three observing periods from summer 2005 through summer 2007. Table 1 shows the sample of galaxies with their coordinates and the rest frequencies of the observed molecular transitions. Observations were performed in symmetrical wobbler switched mode with a frequency of 0.5 Hz and a beam throw of 4' in azimuth. As spectrometers we used the  $512 \times 1$  MHz filter banks for the 3 mm transitions and the  $256 \times 4$  MHz filter banks for those at 2 and 1.3 mm. Pointing accuracy was estimated to be of  $\sim 3''$  from frequent continuum cross scans on nearby pointing sources. Data were calibrated using the standard dual load system and main beam temperatures were obtained as  $T_{\text{MB}} = (F_{\text{eff}}/B_{\text{eff}})T_{\text{A}}^*$ , where  $B_{\text{eff}}$  is tabulated in Table 1 and  $F_{\text{eff}}$  are 0.95, 0.93, and 0.91 for 3, 2, and 1.2 mm, respectively. Calibration uncertainties are estimated to be  $< 15\%$ .

The observed spectra for each source are shown in Fig. 1. The HNCO 5 – 4 and 10 – 9 lines were observed simultaneously with the C<sup>18</sup>O 1 – 0 and 2 – 1 lines, respectively. This allows a reliable determination of the HNCO relative abundance, as no uncertainties due to pointing drifts and/or calibration are involved. For some of the sources with the larger observed linewidths, the HNCO and C<sup>18</sup>O lines appear moderately blended. Such is the case of NGC 7469, NGC 1068, and Arp 220. Gaussian shapes have been fitted to the observed profiles. Table 2 compiles the derived fitted parameters. For the non-detected transitions, upper limits are tabulated where it was considered a  $3\sigma$  level and an approximate linewidth similar to those of the detected CS and HNCO transitions, or that of C<sup>18</sup>O in the case of NGC 5194.

Rotational temperatures and molecular column densities have been derived assuming local thermodynamic equilibrium (LTE) and optically thin emission. As derived for CS  $J = 3 - 2$  in NGC 253 (Martín et al. 2005) we only might expect the emission of CS  $J = 5 - 4$  to be significantly optically thick. However, our observation of C34S will be less affected by the opacity effects. We have accounted for the dilution of the source in the telescope beam by assuming an averaged emission extent of  $10''$  for all sources. This simplification might affect the determination of the column densities for sources much smaller than  $10''$

(see Martín et al. 2006b), but the abundance ratios between species dealt with in this paper (Sect. 4.2) will not be significantly affected. Thus, the main source of uncertainty will be due to possible different emission extents between molecules. Table 3 shows the column density and rotational temperature derived for every source and species. From the LTE analysis, we derive C<sup>18</sup>O rotational temperatures ( $T_{\text{rot}}$ ) of 3 – 7 K for most of the galaxies except for M 82 where we determine  $T_{\text{rot}}=15$  K. The temperatures derived from the HNC O line emission of 4 – 18 K are a factor of  $\sim 2$  higher than those derived from C<sup>18</sup>O. Whenever only one transition was observed, the average rotational temperature of 10 K was assumed.

We have also included the available observations towards NGC 253 to derive its physical parameters shown in Table 3 (Harrison et al. 1999; Martín et al. 2005; Martín et al. 2006b). Note that the C<sup>18</sup>O transitions in NGC 253 were observed  $\sim 10''$  north of the position shown in Table 1. For NGC 4945 we used the observations by Wang et al. (2004). Not all sources in the sample were observed in the CS  $J = 5 - 4$  transition. The upper limit to the emission to this transition in NGC 6946 (Mauersberger et al. 1989) allows to constrain the CS column density to  $< 6.2 \times 10^{13} \text{cm}^{-2}$ . We have thus used the CS  $J = 3 - 2$  transitions available on NGC 6946 and NGC 5194 (Mauersberger et al. 1989) to estimate the column densities presented in Table 3. Note that for NGC 6946 we used the observed offset ( $\Delta\alpha = 10''$ ,  $\Delta\delta = -10''$ ) position in Mauersberger et al. (1989), which is located just  $\sim 1''$  away from our nominal position. Similarly, their NGC 5194 ( $0'', 0''$ ) position is  $\sim 4''$  away from our observed position.

The critical densities for CS and HNC O transitions observed in this works are expected to be very similar since the Einstein coefficients and collisional cross sections are estimated to be similar (Schöier et al. 2005). Thus, the HNC O/CS ratio should reflect a reliable abundances ratio. In any case, the possible uncertainties introduced by slightly different critical densities will never account for the large difference in the abundance ratios measured in different galaxies. The differences in the derived molecular abundances might also be affected by molecular excitation differences of each individual source. However the detailed multitransition study and LVG modeling of dense gas tracers such as HCN and HCO+ in a sample of galaxies by Krips et al. (2008), shows how for several molecular transitions with similar critical densities, the derived abundances from the line intensities are really determined by real differences in abundances and not by excitation effects. The low excitation temperatures derived from C<sup>18</sup>O indicates that a substantial fraction of the column density will be dominated by relatively low density gas. Since in our diagnostic diagrams in Fig. 3 are normalized to the total column densities derived from C<sup>18</sup>O, changes in the H<sup>2</sup> total column densities will not change the main conclusions of the paper.

### 3. Selected sources

The sample of sources observed in this paper has been selected among the brightest prototypes for the different types of nuclear activity. Their distances and corresponding linear scales are shown Table 1. The sources can be grouped as follows.

#### 3.1. Starburst Galaxies (SBG)

*M 82* and *NGC 253* are the strongest and richest extragalactic molecular sources. These are the archetypes of starburst galaxies housing the two brightest extragalactic IRAS sources (Soifer et al. 1989). *M 82*, as opposed to the young starburst in *NGC 253*, is claimed to be the prototype of evolved starburst. This is supported by its observed chemistry characterized by low abundance of complex molecules such as SiO, CH<sub>3</sub>OH (Mauersberger & Henkel 1993; Martín et al. 2006b) and large abundance of molecular ions like CO<sup>+</sup>, HOC<sup>+</sup>, and H<sub>3</sub>O<sup>+</sup> which are expected to be enhanced in PDRs (Fuente et al. 2005, 2006; van der Tak et al. 2008). In this work we did not observe the central position towards *M 82*, but a position in the north-east molecular complex (hereafter *M 82\**) where most of the photodissociation regions are located as observed in the HCO emission high-resolution maps (García-Burillo et al. 2002). *Maffei 2*, is another well studied starburst spiral galaxy with a high molecular gas concentration in its nuclear region and showing traces of a tidal interaction with a dwarf companion galaxy (Hurt et al. 1996; Mason & Wilson 2004). *M 83* is a nearby face on barred galaxy undergoing strong nuclear starburst likely due to gas inflow along its bar (Petitpas & Wilson 1998; Talbot et al. 1979). *NGC 6946* shows a moderate starburst in its nucleus also claimed to be related to the presence of a bar (Turner & Ho 1983; Schinnerer et al. 2007).

#### 3.2. Active Galactic Nuclei (AGN)

*NGC 1068* is a nearby luminous infrared galaxy (LIRG) prototype of a Seyfert 2 nucleus (Antonucci & Miller 1985). The AGN is enclosed by a circumnuclear starburst ring with 14'' ( $\sim 1$  kpc) radius (Myers & Scoville 1987; Schinnerer et al. 2000). Thus, we have observed two positions in *NGC 1068*. One towards the central AGN and an offset position 0'',  $-14''$  towards a peak of emission within the circumnuclear ring, hereafter *NGC 1068\**, mostly tracing the starburst. *NGC 4945*, being one of the three brightest IRAS point sources, has been the target of some a detailed molecular study by Wang et al. (2004). This nearly edge-on spiral galaxy harbor a heavily obscured Seyfert 2 nucleus (Braatz et al. 1997; Maiolino et al. 1999) also surrounded by a starburst ring (Marconi et al. 2000). *NGC 5194* (*M 51*) is a nearby

grand-design spiral galaxy with a Seyfert 2 nucleus. The proximity of this galaxy as well as its nearly face-on orientation has made it the target of numerous large scale multi-wavelength studies (Scoville & Young 1983; Scoville et al. 2001; Schuster et al. 2007). Its interaction with the companion galaxy NGC 5195 seems to have been the origin of a past period of intense star formation (Thronson et al. 1991; Greenawalt et al. 1998). *NGC 7469*, the only example of Seyfert 1 nucleus in our sample, also shows a circumnuclear star-forming ring of  $3''$  in diameter (Wilson et al. 1991).

### 3.3. UltraLuminous Infrared Galaxies (ULIRG)

*Arp 220* is one of the best studied nearby ULIRGs (Dopita et al. 2005) with more than a 95% of its luminosity radiated at IR/submm wavelengths (Sanders et al. 2003). At a distance of  $D \sim 77$  Mpc ( $z = 0.018$ ) and star formation rates of  $300 M_{\odot} \text{ yr}^{-1}$ , *Arp 220* is often referred as a nearby template of the luminous star-forming galaxies at high- $z$ . *Arp 220* is the result of an advanced merger system with two nuclei separated by  $\sim 1''$  ( $\sim 300$  pc) as seen from near-IR and radio images (Baan & Haschick 1995; Scoville et al. 2000) with an enormous concentration of molecular gas within its central region (a few  $10^9 M_{\odot}$ , Sakamoto et al. 1999).

### 3.4. “Normal”

We refer to *IC 342* as a “normal” galaxy as being the closest spiral galaxies resembling our own Galaxy. It shows a minispiral structure meeting at the inner molecular ring surrounding the central stellar cluster (Ishizuki et al. 1990; Boker et al. 1997; Helfer et al. 2003). Chemical differences have been observed between the gas in the nuclear region, affected by the intense star formation through the radiation from the central cluster, and the molecular material in the spiral structure, mainly affected by shocks (Meier & Turner 2005; Usero et al. 2006). In this work we have observed two positions, one at the central region and the other at the offset position ( $+5''$ ,  $+15''$ ), hereafter *IC 342\**, located just in one of the arms of the minispiral.

## 4. Discussion

### 4.1. C<sup>32</sup>S and C<sup>34</sup>S

We have derived the abundances of CS, C<sup>34</sup>S, and HNC relative to H<sub>2</sub>. In order to estimate the H<sub>2</sub> column density we have used the observed C<sup>18</sup>O emission, assuming a <sup>16</sup>O/<sup>18</sup>O abundance ratio of 150, as derived in NGC 253 (Harrison et al. 1999) and the standard CO/H<sub>2</sub> ratio of 10<sup>-4</sup>.

The CS fractional abundance shows a narrow range of values within  $1 - 3 \times 10^{-9}$ . Similarly the C<sup>34</sup>S abundances are concentrated in the range of  $1 - 5 \times 10^{-10}$ . There are only three exceptions to this trend, namely IC 342\*, Arp 220, and NGC 5194. The abundances of CS observed towards IC 342\* is a factor of 6 below the average in the sample, while the C<sup>34</sup>S abundance is close to the average value. This is explained by the highly concentrated CS emission towards the nuclear region (Meier & Turner 2005) and the almost twice smaller beam size at the CS 5 – 4 transition frequency compared to that at the C<sup>34</sup>S 3 – 2 line (see Table 1). We did not detect neither CS nor C<sup>34</sup>S emission towards NGC 5194. While the C<sup>34</sup>S upper limit is still within the average value obtained for the other galaxies, the limit we derive in the main isotopologue is a factor of 3 below the sample average. On the other hand, the galaxy Arp 220 is observed to have an abundance a factor of  $\sim 5$  over the average in both isotopologues. This points out a real overabundance of CS towards this ULIRG.

Fig. 2 shows the C<sup>32</sup>S/C<sup>34</sup>S abundance ratio versus the fractional abundance of CS. This ratio is calculated with the 1 mm CS 5 – 4 and the 2 mm C<sup>34</sup> 3 – 2 transitions which makes it dependent on the assumed rotational temperature to derive the column densities, and to a lesser extent (up to a 30% for the smallest sources) on the considered source size. However, the ratio derived for NGC 4945 and NGC 253 agree within a factor of 1.5 with the values derived from the complete study of CS by Wang et al. (2004) and Martín et al. (2005), respectively. Although the effects of line opacity have not been taken into account, we can consider the derived C<sup>32</sup>S/C<sup>34</sup>S abundance ratio as a rough representation of the <sup>32</sup>/<sup>34</sup>S isotopic ratio. It appears that almost all the sources in the sample have ratios around  $\sim 10$ , in agreement with those previously derived for NGC 4945 and NGC 253, and well below the value of  $\sim 24$  measured in the Galactic disk (Chin et al. 1996). This result supports the idea of an <sup>34</sup>S overproduction in the nuclei of galaxies by massive stars. Furthermore, we observe this ratio to be independent of the type of nuclear activity, both in AGN and SB dominated galaxies.

## 4.2. CS versus HNC0 abundances

In Fig. 3, we represent the fractional abundances of CS and C<sup>34</sup>S versus those of HNC0. We observe that most of the galaxies in the sample are observed with HNC0 fractional abundances ranging from 10<sup>-9</sup> to 10<sup>-8</sup>, but for two sources, namely NGC 5194 and M 82, showing remarkable low HNC0 abundances. For these sources we derived fractional abundance below the average derived from the rest of galaxies in our sample by a factor of  $\sim 3$  and  $\sim 20$ , respectively.

We do not observe major differences in the derived abundances among the AGNs and SBGs in our sample. This homogeneity suggests that the type of nuclear activity does not play a major role at large scales in the production/destruction of these species in the bulk of the molecular gas. This effect is illustrated by the two positions observed in NGC 1068, where the HNC0 and <sup>34</sup>CS abundances decrease by less than a factor of two from the nuclear AGN to the SB ring. Of course we have to bear in mind that the two regions are not fully resolved by the beam of the IRAM 30 m telescope at these frequencies.

If, as suggested by the observations in the Galactic Center region (Martín et al. 2008), the abundance of these species is mostly driven by the presence of shocks and strong UV radiation fields in the ISM, then the observed differences are likely linked to star formation activity in these galaxies. Significant differences are observed within the galaxies IC 342 and Maffei 2. In IC 342, the HNC0/C<sup>18</sup>O ratio increases towards the position in the minispiral and decreases in the central region where ISM is illuminated by the UV radiation from the central clusters. These chemical differences, smoothed to the 10'' – 20'' single-dish beam size, are much more contrasted in the high-resolution interferometric maps by (Meier & Turner 2005). Although not spatially, we resolve the nuclear region of Maffei 2 by the two velocity components. As seen from the high-resolution maps of <sup>13</sup>CO (Meier et al. 2008) the lower velocity component ( $-100 \text{ km s}^{-1}$ ) is associated to the nuclear and northeastern molecular arm, while the higher velocity component ( $0 \text{ km s}^{-1}$ ) will be mostly associated to the nuclear and southwest molecular arm. We clearly see a difference in the chemistry of both components with an increase of the HNC0 abundance towards the southwest molecular arm of a factor of  $\sim 2$  as well as a decrease of the CS abundance of a factor of 3 – 4. Overall, the HNC0/CS ratio increases by almost an order of magnitude.

We can compare the ratios measured in galaxies with the abundances derived in the central region of the Milky Way (Martín et al. 2008). The vast majority of galaxies show HNC0 abundances intermediate between those found in the shock dominated giant molecular clouds (GMCs) and the Galactic PDR prototypes (see dashed lines in Fig 3). Two sources in our sample, namely M 83 and IC 342\* clearly fall in the range of abundances found in GMCs. On the contrary, M 82 represents the other extreme where HNC0 emis-



sion is utterly vanished. The upper limit to the detection derived after a deep 5.5 hours integration on the HNC0 5 – 4 is an order of magnitude lower than the previous limit to the detection in the central position (Nguyen-Q-Rieu et al. 1991), but still HNC0 remains undetected. Interferometric maps with the BIMA array shows no emission anywhere in the nuclear region of M 82 (Turner & Meier 2008). This non-detection of HNC0 supports the idea that M 82 is highly pervaded by a strong UV photodissociating radiation and depleted of dense molecular as also suggested by the low abundance of CH<sub>3</sub>OH and NH<sub>3</sub> (Mauersberger & Henkel 1993; Takano et al. 2002; Martín et al. 2006a). We would expect to observe a higher abundance of CS in this NE position where photodissociation is claimed to be dominant (García-Burillo et al. 2002). However, we observe just a slightly higher CS abundance than in the whole sample, and not even that if we consider the isotopologue C<sup>34</sup>S. Altogether with M 82, the upper limit to the HNC0 abundance derived for NGC5194 are similar to those derived in the Galactic Center PDRs. Most of the molecular studies of NGC5194 so far are restricted to the emission of CO and HCN (Kohno et al. 1996, and references therein). The results from this work point out the possible similarities between the chemistries of NGC 5194 and M 82, both with very low abundances of HNC0 as compared with the rest of galaxies in this sample. This result agrees with the idea of NGC 5194 being in a post starburst stage after the star formation event triggered by its interaction with NGC 5195 (Greenawalt et al. 1998). Additionally, the HNC0 and CS abundances in NGC 253 and NGC 1068\*, a factor of 3 below the average, as well as the significantly high C<sup>34</sup>S abundance, could be explained by photodissociation. This would suggest that the UV radiation from the evolved SB plays a significant role in the chemistry of the nuclear ISM in these galaxies. Therefore NGC 253 would contain a significant PDR molecular component, similar to what is observed in M 82. However, the amounts of dense molecular gas shielded from the UV radiation is still one order of magnitude larger than that observed in M 82.

Our observations of HNC0 confirm that this molecule is one of the best tracers to study the evolutionary state of nuclear starbursts in galaxies because of the high contrast shown between the UV pervaded evolved starbursts and the dense and well shielded molecular material in the early stages of star formation. This molecule shows a higher abundance variation in galaxies than other dense molecular gas tracer such as methanol (Hüttemeister et al. 1997; Martín et al. 2006a). On the other hand, CS does not show a significant variation among the observed sources. This might be due to the fact of CS is not only enhanced in regions with strong UV radiation, but its emission also increases towards the densest molecular cores due to its high critical density. It is interesting to note that the similar FUV field derived by Kramer et al. (2005) towards the nucleus of M 83 and NGC 5194 might explain the different abundances observed in our sample mostly as a consequence of the dense molecular fuel depletion and the molecular cloud structure in their nuclei, and not so much by the differences

in the photodissociation fields affecting the nuclear ISM. However, the CS variations in the Galactic center clouds are more moderate (a factor of  $\sim 2 - 3$ , Martín et al. 2008) than those of HNC, and therefore it is likely to be averaged out over the central several hundred parsecs covered by the single dish beam.

### 4.3. The evolution of nuclear starbursts

The highly contrasted variation of HNC abundances over the galaxy sample in this work allows us to trace the dense molecular gas available for fueling the nuclear starburst of these galaxies. This is equivalent to defining a chemical timeline in the evolution of the starburst event that could be read from right to left hand side in Fig. 3. It is important to note that the time scales for the chemical processes due to shocks and photodissociation by UV radiation ( $10^4 - 10^5$  yr, Bergin et al. 1998) are extremely short as compared with the typical time scale of the starburst phenomenon ( $10^7 - 10^8$  yr, Coziol 1996).

In this scenario, at the onset of the starburst, large amounts of dense molecular material are driven and compressed into the nuclear region of the galaxy unleashing the star formation. High abundances of HNC are injected into the gas-phase within these clouds due to shocks, likely as a consequence of the cloud-cloud collisions, as observed in the nuclear spiral arms of IC 342 (Meier & Turner 2005). From our galaxy sample, M83 is shown to have the highest abundances of HNC, and similar to those observed in the Galactic center GMCs. Subsequently, as soon as the first newly massive star clusters are formed, UV illumination begins to come on stage, photodissociating the material surrounding them. The HNC abundance in these regions will be quickly dissociated where the CS molecule will be formed. A sort of average equilibrium will be reached between the PDR and the dense gas contribution as long as the infall of molecular fuel keeps feeding the starburst. This is the status in which most of the starburst galaxies in our sample are observed. The AGN dominated galaxies we have observed also show this average CS/HNC abundances similar to the intermediate state starbursts, suggesting the presence of a significant UV radiation field. Once the galaxy gets closer to the end the short few 10 Myr starburst period, the fuel supply is cut off or stopped by superwinds. From our comparative study, this is apparently the point at which NGC 253 stands, where photodissociation becomes more important and the fuel reservoir is being consumed by the last gasp of star formation. Finally, as we observe in M82 and NGC 5194, most of the molecular gas is pervaded by the UV radiation field with barely no dense UV shielded molecular material left. The galaxy remains then waiting for a likely next burst of star formation (Coziol 1996). Indeed, chemical enrichment in M82 points out to recursive starburst periods (Origlia et al. 2004).

## 5. Conclusions

From our study of the CS and HNC abundances in a selected sample of extragalactic sources, we have found differences of nearly two orders of magnitude in the HNC/CS abundance ratios among the starburst galaxies. These differences are in agreement with the results from the observations of Galactic center clouds dominated by various heating mechanisms suggesting that the observed HNC abundances could be related to the evolutionary stage of their nuclear starburst. Shocks affecting the massive dense molecular clouds in the early stages and strong UV fields in the evolved stages dominate the HNC abundance in galaxies. We do not find significant differences in the molecular abundances of HNC in galaxies with different type of nuclear activity (i.e. AGN or SB) which implies this species are not affected differently by these processes at the scales observed by single dish beam telescopes.

As derived from the HNC abundances we can point out prototypes of these nuclear starburst evolutionary stages. M83 and the nuclear spiral arms in IC 342 would be representative of the early stage, while M82 and NGC 5194 nuclei would be in the later stages of evolution. NGC 253, claimed to be a prototype of early starburst, shows abundances below the average suggesting an important influence of photodissociation in the heating of its ISM, and therefore chemically closer to M82 than to M83.

The  $^{32}\text{S}/^{34}\text{S}$  isotopic ratio, derived from the  $\text{C}^{32}\text{S}/\text{C}^{34}\text{S}$  abundance ratio, is found to be  $\sim 10$ , and thus similar for all the observed sources. This ratio, found to be well below the value of  $\sim 24$  in the Galactic disk, supports the idea of the  $^{34}\text{S}$  isotope being enriched due to massive star formation events in the nuclear region of galaxies.

The CS emission is suggested to be a good tracer of the molecular gas affected by photodissociation in the Galactic center (Martín et al. 2008). We do not observe a significant contrast in our sample. Though its abundance is enhanced in UV radiated regions, its emission is also favored in high density molecular clouds. Thus the overall emission over the central few hundred parsecs of galactic nuclei is averaged out, and no significant trends in the CS abundances is found in the observed galaxies.

This work has been partially supported by the Spanish Ministerio de Educación y Ciencia under projects ESP 2004-00665 and ESP2007-65812-C02-01, by the Spanish Ministerio de Ciencia e Innovación under project AYA2005-07516-C02-02 and by the “Comunidad de Madrid” Government under PRICIT project S-0505/ESP-0237 (ASTROCAM).

*Facilities:* IRAM 30m

## REFERENCES

- Aalto, S., Polatidis, A. G., Hüttemeister, S., & Curran, S. J. 2002, *A&A*, 381, 783
- Aalto, S., Spaans, M., Wiedner, M.C., & Hüttemeister, S. 2007, *A&A*, 464, 193
- Antonucci, R. R. J., & Miller, J. S. 1985, *ApJ*, 297, 621
- Baan, W. A., & Haschick, A. D. 1995, *ApJ*, 454, 745
- Baan, W. A., Henkel, C., Loenen, A. F., Baudry, A., & Wiklind, T. 2008, *A&A*, 477, 747
- Bergin, E. A., Neufeld, D. A., & Melnick, G. J. 1998, *ApJ*, 499, 777
- Boker, T., Forster-Schreiber, N. M., & Genzel, R. 1997, *AJ*, 114, 1883
- Braatz, J. A., Wilson, A. S., & Henkel, C. 1997, *ApJS*, 110, 321
- Chin, Y.-N., Henkel, C., Whiteoak, J.B., Langer, N., & Churchwell, E.B. 1996, *A&A*, 305, 960
- Coziol, R. 1996, *A&A*, 309, 345
- Dopita, M. A., et al. 2005, *ApJ*, 619, 755
- Fuente, A., García-Burillo, S., Gerin, M., Teyssier, D., Usero, A., Rizzo, J. R., & de Vicente, P. 2005, *ApJ*, 619, L155
- Fuente, A., García-Burillo, S., Gerin, M., Rizzo, J. R., Usero, A., Teyssier, D., Roueff, E., & Le Bourlot, J. 2006, *ApJ*, 641, L105
- García-Burillo, S., Martín-Pintado, J., Fuente, A., Usero, A., & Neri, R. 2002, *ApJ*, 575, L55
- Goicoechea, J. R.; Pety, J.; Gerin, M. et al. 2006, *A&A*, 456, 565
- Greenawalt, B., Walterbos, R. A. M., Thilker, D., & Hoopes, C. G. 1998, *ApJ*, 506, 135
- Harrison, A., Henkel, C., & Russell, A. 1999, *MNRAS*, 303, 157
- Helfer, T. T., Thornley, M. D., Regan, M. W., Wong, T., Sheth, K., Vogel, S. N., Blitz, L., & Bock, D. C.-J. 2003, *ApJS*, 145, 259
- Hurt, R. L., Turner, J. L., & Ho, P. T. P. 1996, *ApJ*, 466, 135
- Hüttemeister, S., Mauersberger, R., & Henkel, C. 1997, *A&A*, 326, 59

- Ishizuki, S., Kawabe, R., Ishiguro, M., Okumura, S. K., & Morita, K.-I. 1990, *Nature*, 344, 224
- Kramer, C., Mookerjea, B., Bayet, E., Garcia-Burillo, S., Gerin, M., Israel, F. P., Stutzki, J., & Wouterloot, J. G. A. 2005, *A&A*, 441, 961
- Kohno, K., Kawabe, R., Tosaki, T., & Okumura, S. K. 1996, *ApJ*, 461, L29
- Kohno, K., Matsushita, S., Vila-Vilaró, B., Okumura, S. K., Shibatsuka, T., Okiura, M., Ishizuki, S., & Kawabe, R. 2001, *ASP Conference Proceedings Vol. 249: “The Central Kiloparsec of Starbursts and AGN: The La Palma Connection”*, 672
- Kohno, K. 2005, *AIP conference proceedings 783 “The evolution of Starburst: The 331st Wilhelm and Else Heraeus Seminar”*, 203
- Krips, M., Neri, R., García-Burillo, S., Martín, S., Combes, F., Graciá-Carpio, J., & Eckart, A. 2008, *ApJ*, 677, 262
- Maiolino, R., Risaliti, G., & Salvati, M. 1999, *A&A*, 341, L35
- Marconi, A., Oliva, E., van der Werf, P. P., Maiolino, R., Schreier, E. J., Macchetto, F., & Moorwood, A. F. M. 2000, *A&A*, 357, 24
- Martín, S., Mauersberger, R., Martín-Pintado, J., García-Burillo, S., & Henkel, C. 2003, *A&A*, 411, L465
- Martín, S., Martín-Pintado, J., Mauersberger, R., Henkel, C., & García-Burillo, S. 2005, *ApJ*, 620, 210
- Martín, S., Martín-Pintado, J., Mauersberger, R. 2006a, *A&A*, 450 L13
- Martín, S., Mauersberger, R., Martín-Pintado, J., & Henkel, C., García-Burillo, S. 2006b, *ApJS*, 164, 450
- Martín, S., Requena-Torres, M. A., Martín-Pintado, J., & Mauersberger, R. 2008, *ApJ*, 678, 245
- Mason, A. M., & Wilson, C. D. 2004, *ApJ*, 612, 860
- Mauersberger, R., Henkel, C., Wilson, T.L., & Harju, J. 1989, *A&A*, 226, L5
- Mauersberger, R. & Henkel, C. 1993, *Rev. Modern Astron.* 6, 69
- Mauersberger, R., Henkel, C., Weiß, A., Peck, A.B., Hagiwara, Y. 2003, *A&A*, 403, 561

- Meier, D. S., & Turner, J. L. 2005, *ApJ*, 618, 259
- Meier, D. S., Turner, J. L., & Hurt, R. L. 2008, *ApJ*, 675, 281
- Myers, S. T., & Scoville, N. Z. 1987, *ApJ*, 312, L39
- Nguyen-Q-Rieu, Henkel, C., Jackson, J. M., & Mauersberger, R. 1991, *A&A*, 241, L33
- Origlia, L., Ranalli, P., Comastri, A., & Maiolino, R. 2004, *ApJ*, 606, 862
- Petitpas, G. R., & Wilson, C. D. 1998, *ApJ*, 503, 219
- Rekola, R., Richer, M. G., McCall, M. L., Valtonen, M. J., Kotilainen, J. K., & Flynn, C. 2005, *MNRAS*, 361, 330
- Sakamoto, K., Scoville, N. Z., Yun, M. S., Crosas, M., Genzel, R., & Tacconi, L. J. 1999, *ApJ*, 514, 68
- Sanders, D. B., Mazzarella, J. M., Kim, D.-C., Surace, J. A., & Soifer, B. T. 2003, *AJ*, 126, 1607
- Schinnerer, E., Eckart, A., Tacconi, L. J., Genzel, R., & Downes, D. 2000, *ApJ*, 533, 850
- Schinnerer, E., Böker, T., Emsellem, E., & Downes, D. 2007, *A&A*, 462, L27
- Schöier, F. L., van der Tak, F. F. S., van Dishoeck, E. F., & Black, J. H. 2005, *A&A*, 432, 369
- Schuster, K. F., Kramer, C., Hitschfeld, M., Garcia-Burillo, S., & Mookerjea, B. 2007, *A&A*, 461, 143
- Scoville, N., & Young, J. S. 1983, *ApJ*, 265, 148
- Scoville N. Z. et al., 2000, *AJ*, 119, 991
- Scoville, N. Z., Polletta, M., Ewald, S., Stolovy, S. R., Thompson, R., & Rieke, M. 2001, *AJ*, 122, 3017
- Soifer, B.T., Boehmer, L., Neugebauer, G., & Sanders, D.B. 1989, *AJ*, 98, 766
- Sternberg, A., & Dalgarno, A. 1995, *ApJS*, 99, 565
- Talbot, R. J., Jr., Jensen, E. B., & Dufour, R. J. 1979, *ApJ*, 229, 91
- Takano, S., Nakai, N., & Kawaguchi 2002, *PASJ*, 54, 195

- Thronson, H. A., Jr., Rubin, H., & Ksir, A. 1991, *MNRAS*, 252, 550
- Turner, J. L., & Ho, P. T. P. 1983, *ApJ*, 268, L79
- Turner, J. L., & Meier, D. S. 2008, *Ap&SS*, 313, 267
- Usero, A., García-Burillo, S., Martín-Pintado, J., Fuente, A., & Neri, R. 2006, *A&A*, 448, 457
- van der Tak, F. F. S., Aalto, S., & Meijerink, R. 2008, *A&A*, 477, L5
- Wang, M., Henkel, C., Chin, Y.-N., Whiteoak, J. B., Hunt Cunningham, M., Mauersberger, R., & Muders, D. 2004, *A&A*, 422, 883
- Wilson, A. S., Helfer, T. T., Haniff, C. A., & Ward, M. J. 1991, *ApJ*, 381, 79
- Zinchenko, I., Henkel, C., & Mao, R.Q. 2000, *A&A*, 361, 1079

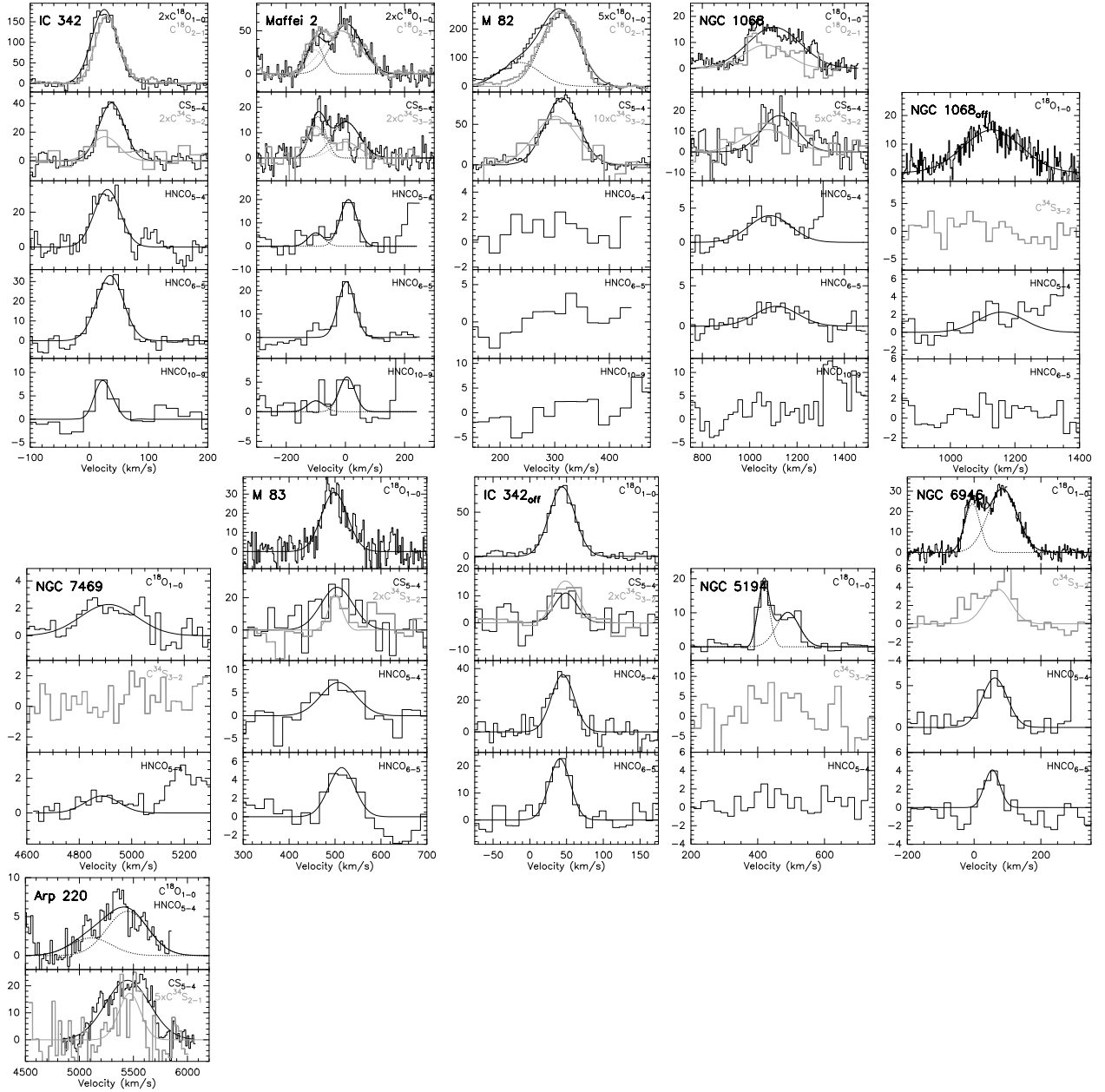


Fig. 1.— Observed spectra for each source in the sample. Some of the transitions  $C^{18}O$  1–0 and  $C^{34}S$  3–2 spectra have been scaled up for the sake of clarity in the profile comparison. Spectra with line intensities below 10 mK have been resampled to a velocity resolution of  $20 \text{ km s}^{-1}$ , otherwise original velocity resolution is shown.  $C^{34}S$  (3–2) in NGC 1068 and  $C^{34}S$  (2–1) in Arp 220 are shown with a  $30 \text{ km s}^{-1}$  velocity resolution. Gaussian fits are shown for all detected transitions. Dotted fits indicate individual velocity components. For Arp 220, where  $C^{18}O$  and HNC O transitions appear significantly blended, we show both fits in the same spectrum where the overall fit is shown with a continuous line and the individual transition with dotted lines. Temperature scale is  $T_{MB}$  (mK).



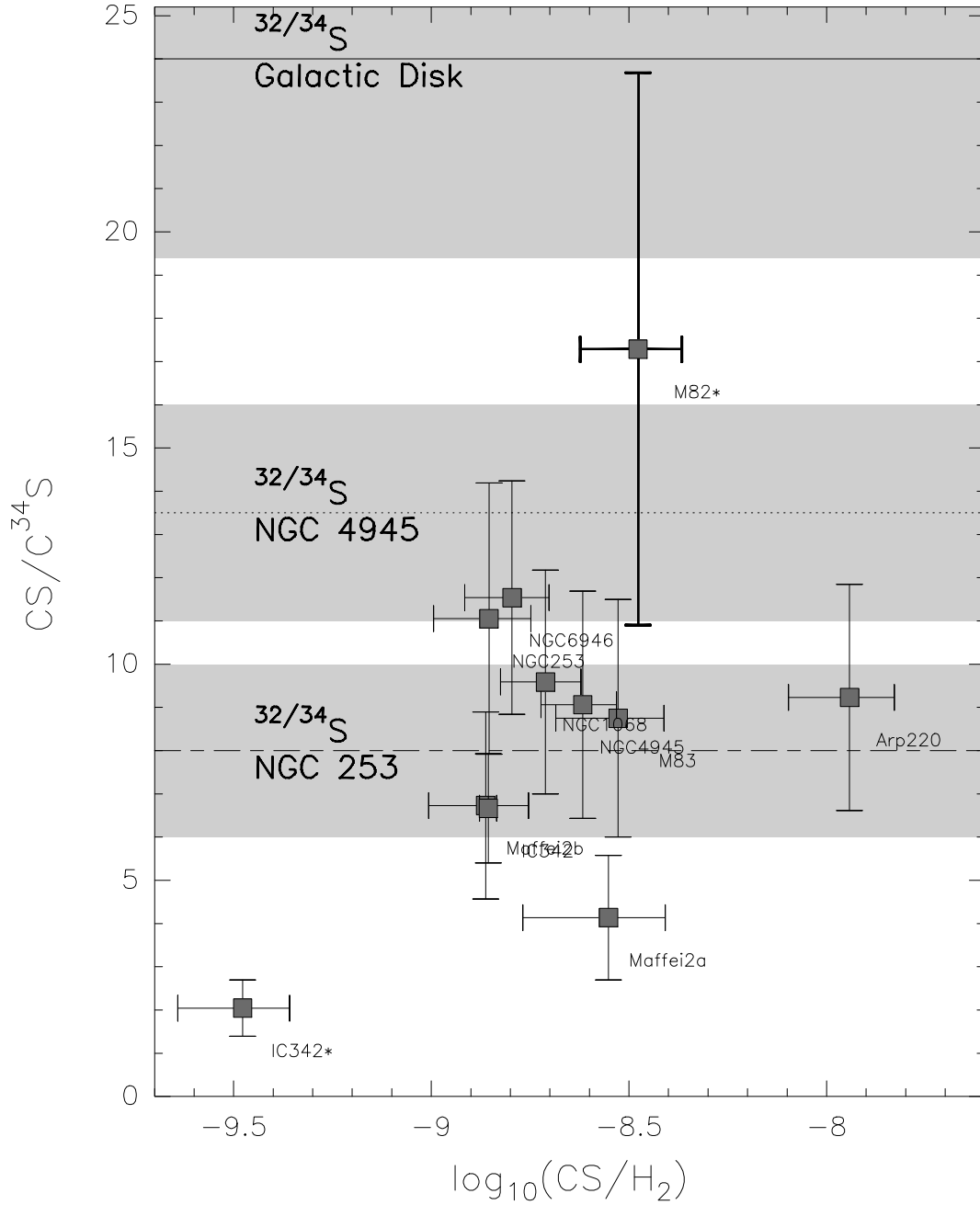


Fig. 2.—  $C^{32}S/C^{34}S$  Abundance ratio for the detected galaxies as a function of the CS fractional abundance. Sulfur isotopic ratios from the literature for the Galactic Disk, and the galaxies NGC 4945 and NGC 253 are represented with continuous, dotted and dashed lines, respectively, and their corresponding error shown as a grey shade. Labeling of sources is the same as in Fig. 3.

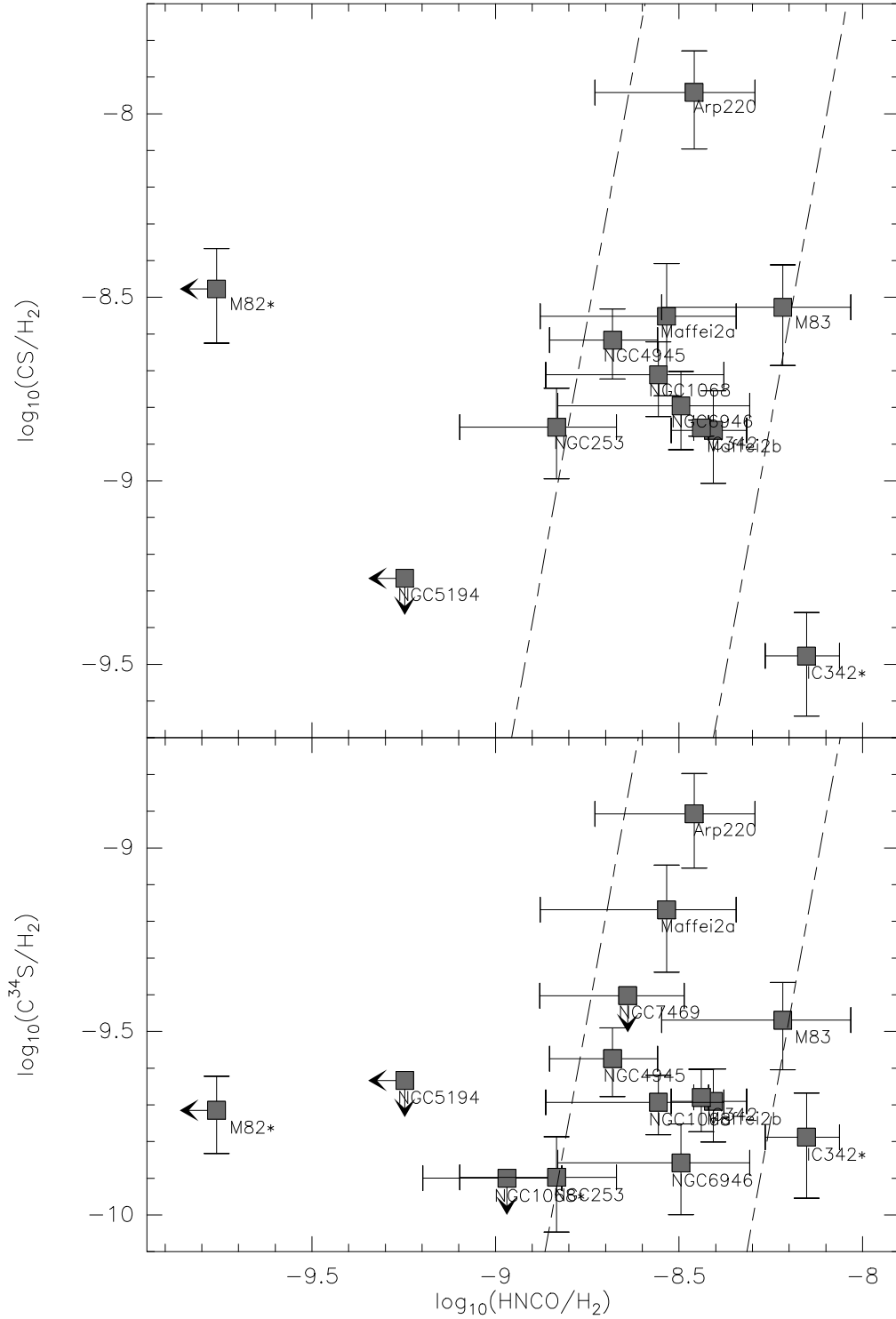


Fig. 3.— Fractional abundances of CS (*Top*) and  $C^{34}S$  (*Bottom*) vs the fractional abundance of HNC/O with respect to  $H_2$ . Upper limits to the abundances are represented by arrows. As in the text, offset observed position are labeled with an \* following the galaxy name. The two velocity components fitted in Maffei2 are labeled as Maffei2a and Maffei2b. Dashed lines represent the limits of the regions used to discriminate the UV dominated (left side) from the shock dominated (right side) molecular gas, as derived from Galactic center observations (see Martín et al. 2008, for details).

Table 1: Observational parameters

SOURCE SAMPLE			
Source	$\alpha_{J2000}$	$\delta_{J2000}$	$D_{L/A}$ (Mpc–pc/'') <sup>a</sup>
<i>NGC 253</i>	00:47:33.3	-25:17:23	2.5 – 12
Maffei 2	02:41:55.2	59:36:11	5.0 – 24
NGC 1068 <sup>b</sup>	02:42:40.9	-00:00:46	16.7 – 81
IC 342 <sup>c</sup>	03:46:48.6	68:05:46	3.7 – 18
M 82 <sup>d</sup>	09:55:51.9	69:40:47	3.5 – 17
<i>NGC 4945</i>	13:05:27.2	-49:28:05	7.8 – 38
NGC 5194 (M 51)	13:29:52.7	47:11:43	9.7 – 47
M 83	13:37:00.9	-29:51:56	3.7 – 18
Arp 220	15:34:57.1	23:30:12	73.0 – 354
NGC 6946	20:34:52.4	60:09:14	5.5 – 27
NGC 7469	23:03:15.6	08:52:26	66 – 320
MOLECULAR LINES			
Molecule	Frequency (GHz)	$\Theta_{\text{beam}}$ (") <sup>e</sup>	$B_{\text{eff}}$ <sup>f</sup>
C <sup>18</sup> O $J = 1 - 0$	109.782	22	0.75
C <sup>18</sup> O $J = 2 - 1$	219.560	11	0.55
CS $J = 5 - 4$	244.935	10	0.49
C <sup>34</sup> S $J = 2 - 1$ <sup>g</sup>	96.412	25	0.76
C <sup>34</sup> S $J = 3 - 2$	144.617	17	0.69
HNCO $5_{0,5} - 4_{0,4}$	109.905	22	0.75
HNCO $6_{1,6} - 5_{1,5}$	131.885	19	0.71
HNCO $10_{0,10} - 9_{0,9}$	219.798	11	0.55

Note. — The data for sources in *italics* were taken from previously published data.

<sup>a</sup>Distances as derived by Baan et al. (2008) and linear scales given in parsecs per arcsecond at those distances.

<sup>b</sup>Central and (0'', -16'') offset (NGC 1068\* in the text) positions were observed.

<sup>c</sup>Central and (5'', 15'') offset (IC 342\* in the text) positions were observed.

<sup>d</sup>Central position was not observed, but the NE molecular lobe at the approximate offset (13'', 7.5'') position, referred to as M 82\* in the text.

<sup>e</sup>All data are from the IRAM 30 m telescope, but for those of NGC 4945 from SEST (Wang et al. 2004). In this case, the beam is about twice the given size.

<sup>f</sup>Beam efficiency of the IRAM 30 m at the observed frequencies

<sup>g</sup>This transition is only observed towards Arp 220.

Table 2: Parameters derived from the Gaussian profiles fitted to the observations.

Transition	$\int T_{\text{mb}} dv$ (K km s <sup>-1</sup> )	$v_{\text{LSR}}$ (km s <sup>-1</sup> )	$\Delta v_{1/2}$ (km s <sup>-1</sup> )	$T_{\text{MB}}$ (mK)	$rms^a$ (mK)
<b>Maffei 2</b>					
C <sup>18</sup> O 1 – 0	1.2 ± 0.2	-102 ± 4	63 ± 7	18.2	1.9
	3.7 ± 0.3	4 ± 4	120 ± 10	29.0	
C <sup>18</sup> O 2 – 1	2.0 ± 0.2	-102.2 ± 1.4	66 ± 3	28.0	1.0
	8.0 ± 0.2	-14 ± 2	151 ± 4	49.8	
CS 5 – 4	1.1 ± 0.2	-93 ± 4	63 ± 9	16.3	1.4
	1.7 ± 0.3	2 ± 10	110 ± 20	14.3	
C <sup>34</sup> S 3 – 2	0.41 ± 0.08	-100	65	6.0	1.4
	0.37 ± 0.12	0	110	3.2	
HNCO 5 – 4	0.38 ± 0.10	-100	62	5.8	2.1
	1.42 ± 0.13	10 ± 3	66 ± 7	20.1	
HNCO 6 – 5	< 0.3		65	< 5.0	2.5
	1.67 ± 0.17	4 ± 3	66 ± 8	23.9	
HNCO 10 – 9	0.13 ± 0.06	-100	65	1.8	1.0
	0.39 ± 0.06	5 ± 6	62 ± 10	5.9	
<b>NGC 1068</b>					
C <sup>18</sup> O 1 – 0	4.45 ± 0.12	1102 ± 4	264 ± 8	15.8	0.8
C <sup>18</sup> O 2 – 1	2.0 ± 0.2	1067 ± 12	210 ± 30	9.0	1.9
CS 5 – 4	3.3 ± 0.3	1125 ± 9	180 ± 20	17.6	3.0
C <sup>34</sup> S 3 – 2	0.53 ± 0.12	1070 ± 30	230 ± 60	2.2	1.0
HNCO 5 – 4	0.86 ± 0.09	1086 ± 11	210 ± 20	3.9	0.8
HNCO 6 – 5	0.56 ± 0.07	1114 ± 13	210 ± 30	2.5	0.6
HNCO 10 – 9	< 0.4		210	< 2.1	1.9
<b>NGC 1068 (0'', -16'')</b>					
C <sup>18</sup> O 1 – 0	3.39 ± 0.14	1130 ± 4	213 ± 10	15.0	1.1
C <sup>34</sup> S 3 – 2	< 0.2		170	< 1.4	1.2
HNCO 5 – 4	0.41 ± 0.11	1160 ± 20	170 ± 40	2.3	1.1
HNCO 10 – 9	< 0.2		170	< 1.0	0.8
<b>IC 342 (0'', 0'')</b>					
C <sup>18</sup> O 1 – 0	4.80 ± 0.11	25.2 ± 0.6	50.1 ± 1.2	89.9	1.7
C <sup>18</sup> O 2 – 1	8.10 ± 0.10	29.9 ± 0.3	46.3 ± 0.6	164.1	1.1
CS 5 – 4	2.15 ± 0.11	37.7 ± 1.2	50 ± 3	40.3	1.8
C <sup>34</sup> S 3 – 2	0.49 ± 0.12	26 ± 7	54 ± 12	8.4	1.5
HNCO 5 – 4	1.81 ± 0.10	30.5 ± 1.4	52 ± 3	33.0	1.7
HNCO 6 – 5	1.87 ± 0.11	35.0 ± 1.6	53 ± 3	33.0	1.9
HNCO 10 – 9	0.31 ± 0.06	24 ± 3	34 ± 8	8.5	1.1
<b>IC 342 (5'', 15'')</b>					
C <sup>18</sup> O 1 – 0	3.45 ± 0.10	43.9 ± 0.6	41.1 ± 1.4	78.8	2.0
CS 5 – 4	0.42 ± 0.10	49	36	11.0	2.6
C <sup>34</sup> S 3 – 2	0.32 ± 0.04	49 ± 2	36 ± 6	8.3	1.0
HNCO 5 – 4	1.39 ± 0.10	44.9 ± 1.2	36 ± 3	36.2	2.0
HNCO 6 – 5	0.81 ± 0.10	41 ± 2	34 ± 5	22.7	2.0
<b>M 82</b>					
C <sup>18</sup> O 1 – 0	1.55 ± 0.07	235 ± 2	87 ± 5	16.8	0.7
	4.41 ± 0.06	310	80	51.9	
C <sup>18</sup> O 2 – 1	22.79 ± 0.15	309.5 ± 0.3	81.9 ± 0.6	261.5	2.0
CS 5 – 4	6.4 ± 0.2	313.0 ± 1.0	73 ± 2	82.6	2.5
C <sup>34</sup> S 3 – 2	0.58 ± 0.08	302 ± 6	91 ± 13	6.0	1.0
HNCO 5 – 4	< 0.10		80	< 1.3	0.7
HNCO 6 – 5	< 0.17		80	< 2.3	1.3
HNCO 10 – 9	< 0.3		80	< 3.7	2.0
<b>NGC 5194</b>					
C <sup>18</sup> O 1 – 0	0.80 ± 0.08	418.2 ± 1.4	39 ± 3	19.1	0.6
	0.86 ± 0.09	490 ± 5	80 ± 8	10.1	
C <sup>34</sup> S 3 – 2	< 0.2		100	< 2.2	1.4
HNCO 5 – 4	< 0.11		100	< 1.0	0.6
<b>M 83</b>					
C <sup>18</sup> O 1 – 0	2.19 ± 0.14	499 ± 2	66 ± 5	30.9	1.9
CS 5 – 4	2.3 ± 0.3	504 ± 7	82.4 ± 1.1	26.5	0.5
C <sup>34</sup> S 3 – 2	0.40 ± 0.13	501 ± 6	34 ± 13	11.1	2.7
HNCO 5 – 4	0.70 ± 0.15	510 ± 10	90 ± 19	7.7	1.9
HNCO 6 – 5	0.38 ± 0.07	515 ± 7	67 ± 12	5.4	1.2
<b>Arp 220</b>					
C <sup>18</sup> O 1 – 0	2.7 ± 0.3	5445	450 ± 40	5.7	0.9
CS 5 – 4	11.3 ± 0.2	5446 ± 5	481 ± 11	22.0	2.7
C <sup>34</sup> S 2 – 1	0.9 ± 0.2	5460 ± 30	240 ± 50	3.4	1.4
HNCO 5 – 4	1.1 ± 0.2	5445	450	2.3	0.9
<b>NGC 6946</b>					
C <sup>18</sup> O 1 – 0	1.36 ± 0.10	-5.0 ± 1.4	54 ± 3	23.8	0.7
	3.41 ± 0.11	84.7 ± 1.7	103 ± 4	31.2	
C <sup>34</sup> S 3 – 2	0.37 ± 0.07	71 ± 11	90 ± 20	3.8	0.7
HNCO 5 – 4	0.55 ± 0.10	62 ± 8	87 ± 19	5.9	0.7
HNCO 6 – 5	0.24 ± 0.06	54 ± 7	53 ± 14	4.1	1.0
<b>NGC 7469</b>					
C <sup>18</sup> O 1 – 0	0.61 ± 0.05	4910 ± 10	250 ± 20	2.3	0.4
C <sup>34</sup> S 3 – 2	< 0.13		150	< 0.9	0.6
HNCO 5 – 4	0.16 ± 0.04	4890 ± 20	150 ± 40	1.0	0.4

Table 3: Derived column densities and rotational temperatures for each galaxy.

Source	C <sup>18</sup> O		CS	C <sup>34</sup> S	HNCO	
	( $\times 10^{15} \text{cm}^{-2}$ )	(K)	( $\times 10^{13} \text{cm}^{-2}$ )	( $\times 10^{12} \text{cm}^{-2}$ )	( $\times 10^{13} \text{cm}^{-2}$ )	(K)
NGC 253 <sup>a</sup>	100 ± 20	5.6 ± 0.4	21 ± 4	19 ± 4	22 ± 9	18 ± 4
Maffei 2 <sup>b</sup>	5.7 ± 1.5	5.6 ± 0.6	2.4 ± 0.7	5.8 ± 1.1	2.5 ± 1.2	12.2 ± 1.9
	17 ± 2	6.6 ± 0.3	3.5 ± 0.9	5.2 ± 1.0	10 ± 2	11.5 ± 0.6
NGC 1068	24 ± 2	3.3 ± 0.1	7.0 ± 1.5	7.3 ± 1.2	10 ± 5	5.8 ± 0.8
NGC 1068*	18 ± 4	...	...	< 3.4	2.9 ± 1.0	...
IC 342	22 ± 1	5.7 ± 0.1	4.6 ± 0.1	6.9 ± 1.3	12 ± 1	10.2 ± 0.4
IC 342*	18 ± 4	...	0.9 ± 0.2	4.4 ± 1.0	19 ± 1	5.3 ± 0.6
M 82*	28 ± 1	14.5 ± 0.3	14 ± 4	8.1 ± 1.9	< 0.7	...
NGC 4945 <sup>c</sup>	160 ± 10	6.5 ± 0.2	58 ± 12	64 ± 13	50 ± 16	...
NGC 5194	8.6 ± 1.8	...	< 0.7 <sup>d</sup>	< 3.0	< 0.7	...
M 83	11 ± 2	...	4.9 ± 1.2	5.6 ± 1.1	10 ± 5	5.0 ± 1.1
Arp 220	14 ± 3	...	24 ± 5	26 ± 5	7 ± 3	...
NGC 6946	25 ± 5	...	6.0 ± 0.8 <sup>d</sup>	5.2 ± 1.0	12 ± 6	4.2 ± 0.9
NGC 7469	3.2 ± 0.7	...	...	< 1.9	1.1 ± 0.4	...

\* Indicates offset positions.

<sup>a</sup> Derived using data from Harrison et al. (1999); Martín et al. (2005); Martín et al. (2006b).

<sup>b</sup> Abundances derived for each of the two velocity components labeled as Maffei 2a and Maffei 2b in Fig. 3.

<sup>c</sup> Derived using data from Wang et al. (2004).

<sup>d</sup> Derived using data from Mauersberger et al. (1989).